M. S. DISSERTATION

EFFECT OF THERMAL ANNEALING ON PERFORMANCE OF INVERTED INDIUM PHOSPHIDE QUANTUM DOTS LIGHT-EMITTING DIODES

열처리가 인화인듐 양자점 발광 다이오드의
성능에 미치는 영향에 대한 연구

February 2019

DEPARTMENT OF
ELECTRICAL AND COMPUTUER ENGINEERING
COLLEGE OF ENGINEERING
SEOUL NATIONAL UNIVERSITY

JIWON LEE

EFFECT OF THERMAL ANNEALING ON PERFORMANCE OF INVERTED INDIUM PHOSPHIDE QUANTUM DOTS LIGHT-EMITTING DIODES

열처리가 인화인듐 양자점 발광 다이오드의 성능에 미치는 영향에 대한 연구

지도 교수 홍용택

이 논문을 공학석사 학위논문으로 제출함

2019년 2월

서울대학교 대학원
전기정보공학부
이지원

이지원의 공학석사 학위논문을 인준함

2019년 2월

위 원 장 정윤찬 (인)
부위원장 홍용택 (인)
위 원 이창희 (인)

Abstract

JIWON LEE
DEPARTMENT OF ELECTRICAL AND
COMPUTER ENGINEERING
COLLEGE OF ENGINEERING
SEOUL NATIONAL UNIVERSITY

Indium phosphide (InP) quantum-dots (QDs) have attracted as the most prospective luminescent material for developing cadmium-free QD light-emitting diodes (QLEDs). However, the performance including efficiency, maximum luminance and operational lifetime of InP QLEDs is still far behind that of CdSe QLEDs. This is mainly attributed to unoptimized nanostructures of InP QDs and devices. InP QDs have relatively low electron affinity (EA), so the electron injection barrier is quite large with conventionally available electron transporting materials, thereby resulting in low electron injection. In this study, I demonstrate that simply thermal annealing of zinc oxide nanoparticle (ZnO NPs) electron transport layer and the QD emissive layer can lead to enhanced QLED performance without complicating device fabrication process. The current density of electron-only devices with ZnO NPs increases and exhibits trap-free space-charge-limited-current (TFSCLC) characteristics after the thermal annealing. It is attributed to the reduced oxygen vacancies of ZnO NPs, which act as scattering sites. Furthermore, the photoluminescence (PL) intensity of the InP QD thin films increases by thermal annealing due to alleviated trap states and increased packing density of InP QDs, as previously reported. Optimizing annealing temperature of inverted green InP QLEDs results in increased external quantum efficiency

from 2.32% to 3.61% and maximum brightness over 10,000 cd/m^2. The half-lifetime (T_{50}) at an initial luminance of 1000 cd/m^2 increases up to nearly 2 hours, which corresponds to 62.0 h at initial luminance of 100 cd/m^2, which is the longest lifetime of academically reported InP QLEDs so far. This thesis proposes thermal annealing process as a simple and effective process to further optimize the device performance of InP QLEDs.

Keyword : Indium Phosphide quantum dots, Quantum dots light-emitting diodes, Annealing, Zinc Oxide nanoparticles, Oxygen vacancy, Charge balance
Student Number : 2017-28685

Contents

List of Figures

List of Tables

Chapter 1

Introduction

1.1 Cadmium-Free Quantum Dot Light-Emitting Diodes

Quantum dot light-emitting diodes (QLEDs) are very prospective light-emitting devices which are expected to outperform organic light-emitting diodes (OLEDs) since colloidal quantum dots (QDs) have superior luminescent properties than any other luminescent organic molecules. From the start of QLEDs by A. P. Alivisatos group[1], QLEDs have been significantly advanced with great amount of studies. The world-record external quantum efficiencies (EQEs) of red, green and blue single-unit QLEDs reached so far are, 20.5 %[2], 21.0%[3] and 19.8%[4], correspondingly. The highest device half-lifetime (T_{50}), another important factor of QLEDs to be commercialized, of red, green and blue QLEDs are respectively 1,330,000 h[5], 76,000 h[6] and 1,000 h[7] at initial luminance of 100 cd/m^2. Blue-emitting QLEDs have relatively short lifetimes, but they are expected to be improved significantly in the near future, considering the rapid advances of structural engineering of QDs and devices.

Although record-breaking EQE and device lifetime of QLEDs are steadily reported so far, the main limitation still remains. Most of the achievements are based on toxic Cd-containing QDs. Following the worldwide trend of environmental friendliness, the usage of Cd in electronics are tightly regulated. For instance, European Union has been limited the Cd content by the Restriction of Hazardous Substances (RoHS) directives. Cd-free QDs and QLEDs are actively studied recently by academic research groups and companies in this regards. The representative Cd-free QDs are InP[8-20] (III-V), ZnSe[21-25] (II-VI), CuInS[26-33] and AgInS[34-36] (I-III-VI) QDs. Among these, the most spotlighted one for display application is InP QDs. InP QDs exhibit efficient band-edge emission, so the spectral purity can be controlled as narrow as CdSe QDs, with full width at half maximum (FWHM) on the order of 40 nm. More importantly, InP QDs have wide spectral range from red[12] to blue[18], which make InP QDs suitable for display application.[8] ZnSe QDs, on the other hand, are limited to blue emitters because of the intrinsically wide bandgap of ZnSe.[24] I-III-VI QDs are rather suitable for solid-state lighting (SSL) application due to broad PL bandwidth on the order of 100 nm, originating from efficient intragap emission via two distinct oxidative state of Cu.[37] Several studies showed that colors can be tuned by varying chemical composition[26, 31, 35], but the color range of I-III-VI QDs are confined from red to green up till now. The performances of Cd-free QLEDs with each type of QDs are poorer than CdSe QLEDs so far but are getting improved by many researchers with the accumulated knowledge of CdSe QLEDs.

1.2 Nanostructure and Device Engineering of QLEDs

Based on the knowledge of device operation and origins of low efficiency and stability, several approaches have been investigated. Such studies can be divided into nanostructure engineering of QDs and device engineering of QLEDs.

The origins of poor performances of the early QLEDs have been unveiled by several research groups. It is widely accepted that the key limiting factor of QLEDs is imbalance of electron transport and hole transport. From the expression of EQE described in Equation 1.1, EQE can be decomposed into four components: charge balance factor (γ), exciton generation factor (η_{ex}), effective quantum yield (η_{PL}^{*}) and outcoupling (light-extraction) factor (η_{oc}). Charge imbalance reduces EQE with respect to charge balance factor (γ) and effective quantum yield (η_{PL}^{*}). Charge imbalance causes QD charging and generates charged excitons. Charged exciton (positive trion, negative trion and multiply charged exciton) has multifold lower quantum yield η_{PL}^{*} than neutral electron-hole paired exciton, which is attributed to nonradiative Auger recombination.[38]

$$\mathrm{EQE} = \eta_{oc}\gamma\eta_{ex}\eta_{PL}^{*} \tag{1.1}$$

CdSe QDs in general have deep valence band maximum (VBM) (6~7 eV), so low hole injection from commercially available hole transport layers (HTLs) to CdSe QDs has limited the performance of CdSe QLEDs.[39] On the other hand, InP QDs have relatively upshifted energy levels, so electron injection from commercially available electron transport layers (ETLs) to InP QDs is limited in InP QLEDs due to larger electron injection barrier between QDs and ETL than hole injection barrier between QDs and HTL.[8] Researchers have attempted to enhance hole injection/transport for CdSe QLEDs and

electron injection/transport for InP QLEDs in these regards.

The enhancement of QLEDs can be categorized into three aspects: QD structure design, device design and process design. First, QD structure design have focused on high photoluminescence quantum yield (PL QY) of QDs. The two representative approaches, thick-shell QDs[40] and softly alloyed QDs with compositional gradient[41-43] enabled high PL QY of QDs by suppressing charge imbalance and Auger recombination. Recently reported efficient QLEDs were mostly fabricated with thick-shell QDs. On the one hand, ligand exchange could enhance the charge balance.[6, 44-46] Second, sophisticated device design aimed to balance electron transport and hole transport by adjusting energy levels and mobilities of ETLs and HTLs. Several materials have been doped and mixed as charge transport layers (CTLs).[27, 47-54] Third, process-related approaches such as annealing[55-57] and solvent-orthogonality[58] enabled further device improvements with respect to charge balance and processability.

Among above approaches, annealing processes have been rarely reported so far. F. Mizukami's group studied the PL properties of thermally annealed QD-clay composite thin films.[57] A. K. Jen's group fabricated multi-fold enhanced red QLEDs with thermal annealing.[56] Thermal annealing suppressed parasitic organic emission, reduced turn-on voltage, and increased electroluminescence (EL) efficiency and brightness of red CdSe/CdS QLEDs. They attributed these progresses to ligand desorption confirmed by Gas Chromatography Mass Spectrometry (GC/MS) and thermo-gravitational analysis (TGA). The QD emissive layer (EML) could be smoothed as the annealing temperature was higher than the melting transition temperature of QD ligand thereby QDs are ordered. In addition, desorption of QD ligand enhanced charge injection by reducing insulating barrier thickness. These two

mechanisms improved EL efficiency in their work so significantly that cancel out the PL efficiency reduction of the annealed QD thin films due to the loss of surface passivation. C. Han's group observed photoenhancement of QD-polymer composite thin films via UV annealing.[55] They found PL and EL enhancement with the red CdSe/CdS/CdZnS/ZnS QD and QD/polymer nanocomposite thin films, depending on 365 nm-UV irradiation intensity and exposure time. The morphological enhancement of QD thin films as UV annealing was also observed by transmission electron microscopy (TEM) images, but the detailed mechanism of the photoenhancement of QDs are still in mystery.

In this thesis, the effects of thermal annealing on inverted InP/ZnSeS/ZnS QLEDs are investigated. Strong dependence of device efficiency and lifetime on annealing temperature is observed.

1.3 Outline of Thesis

This thesis consists of four chapters.

In Chapter 1 as introduction, origins of low efficiency and stability of quantum dots light-emitting diodes, necessity of cadmium-free quantum dots light emitting diodes, and previous studies for highly efficient and stable quantum dots light emitting diodes are described.

In Chapter 2 as experimental methods, detailed fabrication and characterization methods of QLEDs are given.

In Chapter 3, improved efficiency and lifetime of inverted InP QLEDs as thermal annealing of QDs are demonstrated. The origins of the performance enhancement are discussed in the aspect of conductivity of ZnO nanoparticles, photoluminescence and morphology of QDs.

In Chapter 4 as conclusion, the results are summarized and concluding remarks of this thesis are given.

Chapter 2

Experimental Methods

2.1 Materials

2.1.1 Preparation of ZnO Nanoparticles

ZnO nanoparticles were synthesized modifying the method reported by Pacholski *et al.* [59] 2 g of $Zn(ac)_2 \cdot 2H_2O$ and 80 mL of methanol were first placed in a 3-neck round bottom flask and heated to 60 °C. At 60 °C, a 65 mL KOH solution containing 1.51 g of KOH was added dropwise into the $Zn(ac)_2 \cdot 2H_2O$ solution under strong agitation. The reaction mixture was kept at 60 °C for 2 hr 15 min to yield a milky solution containing ZnO nanoparticles. The ZnO nanoparticles were then isolated by centrifugation at 4000 rpm followed by repetitive washing using methanol. Finally, the product was centrifuged again and re-dispersed in 6 mL of butanol.

2.1.2 Synthesis of Green Color Emitting InP/ZnSeS/ZnS Core/shell Heterostructured Quantum Dots

Modified synthetic procedure by Lim et al. was adopted for the synthesis of InP/ZnSeS QDs. [17] Briefly, 0.1mmol of $InCl_3$ in 1mL of tetrahydrofuran, 2mL of zincoleate ($Zn(OA)_2$, 30 mmol of zinc acetate reacted with 19 mL of oleic acid (OA) under vacuum and diluted with 41 mL of 1-octadecene (ODE)), and

8mL of ODE were loaded in a 100 mL flask with a condenser and degassed for 30 min to remove water and oxygen species. After backfilling the reactor with N_2, temperature was increased to 280 °C and a mixture of 0.1 mmol of $P(TMS)_3$ and 0.4 mmol of STBP (0.4 mmol of sulfur dissolved in 0.5 mL of TBP and 0.5 mL of ODE) was rapidly injected into the reactor. After 20 s, 0.2 mL of SeTOP (0.2 mmol of Se dissolved in 0.5 mL of n-trioctylphosphine and 0.5 mL of ODE) was slowly added for 20 s and reacted at 280 °C for 10 min. Next, 4 mL of $Zn(OA)_2$ and 1.8 mL of 1-dodecanethiol were added and reacted for 90 min at 300 °C. Finally, 6 mL of $Zn(OA)_2$ and 0.72 mL of 1-dodecanethiol were added, and the mixture was reacted for 120 min. After the reaction was terminated, the mixture was cooled to room temperature to terminate the reaction. For the purification of QDs, a precipitation/redispersion method was employed; the crude solution was precipitated with an excess amount of acetone and redispersed with toluene. After repeated purification processes (typically 4 times), the precipitated QDs were dried under N_2 flow for 5 min and dispersed in toluene.

2.1.3 Organic Materials

4,4',4''-tris(N-carbazolyl)-triphenylamine (TCTA) as hole transport layer is purchased from OSM. poly[(9,9-bis(3'-(N,N-dimethylamino)propyl)-2,7-fluorene)-alt-2,7-(9,9-ioctylfluore ne (PFN-P1) as conjugated polyelectrolyte layer was purchased from 1-Material Inc. Chemical structures of organic materials used in this thesis are as follows.

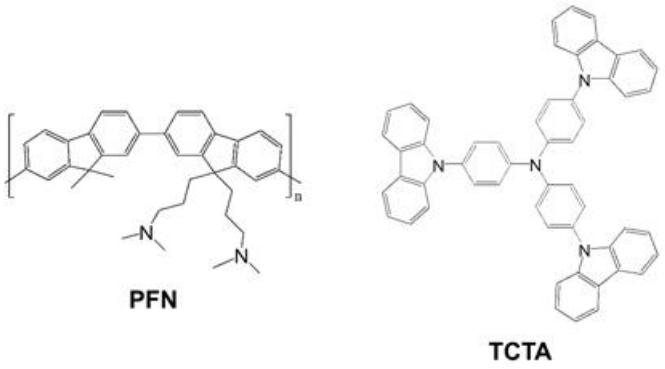

Figure 2.1 Chemical structures of CBP, TCTA and PFN

2.2 Device Fabrication and Characterization Methods

2.2.1 Device Fabrication

A schematic and energy diagram of the QLEDs in this work are shown in Figure 2.2. All QLED devices were fabricated using the inverted architecture with ITO cathode and aluminum anode. The fabrication process is as follows. First, pre-patterned ITO/glass substrates were cleaned with acetone, isopropanol and deionized water in an ultrasonicator (Branson 5510). Then the cleaned ITO/glass substrates were dried in the oven at 120 °C. For the inverted architecture, 20 mg/mL of the ZnO nanoparticle solution dispersed in butanol was spin-coated on the ITO/glass substrates with a spin-rate of 2000 rpm for 40 seconds and dried at 100 °C for 30 min in an oven filled with N_2 gas. The thickness of ZnO nanoparticle layer as electron injection/transport layer was about 40 nm. The substrates were transferred to Ar-filled glovebox (MBRAUN), and 0.5 mg/mL of PFN-P1 solution dispersed in methanol was spin-coated on the substrates at 4000 rpm for 30 seconds and dried in vacuum chamber for 30 minutes. Then 10 mg/ml of green InP/ZnSeS/ZnS QD solution dispersed in toluene was spin-coated on the PFN-P1 layer at 4000 rpm for 30 seconds, followed by drying in vacuum chamber for 20 minutes. To prepare thermal annealed QLEDs, ITO/ZnO/PFN-P1/QD substrates were annealed on hotplate in Ar-filled glovebox for 15 minutes with different temperatures (60, 80, 100, 120 and 150 °C), right after spin-coating of QDs. After drying or thermal annealing of QDs, the substrates were transferred to thermal evaporating deposition system. A vacuum box was used not to expose the substrates into air. 50 nm of TCTA as hole transport layer, 10 nm of MoO_x as hole injection layer and 130 nm of Al anode was deposited at low vacuum level under 10^{-6} Torr.

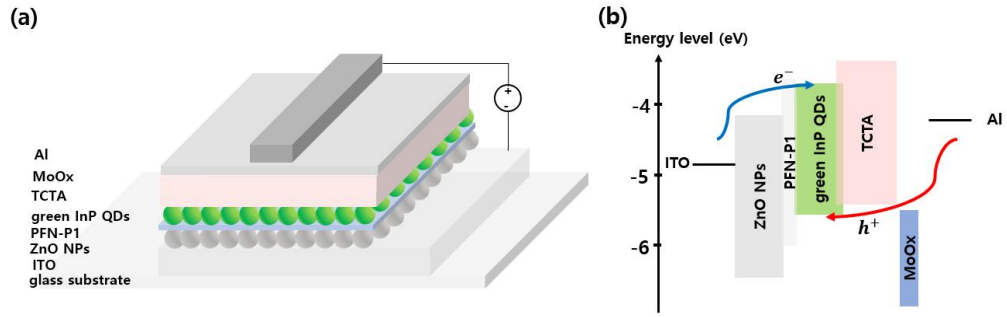

Figure 2.2 Schematic diagrams of (a) device structure and (b) energy-level of the green inverted InP QLEDs

2.2.2 Current-voltage-luminance Measurement

The current-voltage (I-V) characteristics were measured with a Keithley 236 source measurement unit, while the electroluminescence was measured with a calibrated Si photodiode (Hamamatsu, S5227-1010BQ) with a size of 10 mm × 10 mm placed at an angle normal to the device surface, assuming that the device was a Lambertian source. To detect a turn-on voltage of light-emitting diodes, we use an ARC PD438 photomultiplier tube (PMT) with the Keithley 236 source measurement unit. The electroluminescence (EL) spectra and the Commission Internationale de L'Eclairage (CIE) color coordinates were measured with a Konica-Minolta CS-2000 spectroradiometer. The luminance and efficiency were calculated from the photocurrent signal of photodiode with a Keithley 2000 multimeter, and corrected precisely with the luminance from CS-2000.

The chromatic characteristics were calculated from EL spectra measured by the CS-2000 spectrometer using the CIE 1931 color expression system. The tristimulus values XYZ can be calculated by following equations,

$$X = K_m \int_0^\infty \bar{x}(\lambda)P(\lambda)d\lambda \quad (2.1)$$

$$Y = K_m \int_0^\infty \bar{y}(\lambda)P(\lambda)d\lambda \quad (2.2)$$

$$Z = K_m \int_0^\infty \bar{z}(\lambda)P(\lambda)d\lambda \quad (2.3)$$

where, P(λ) is a given spectral power distribution of emissive source, $\bar{x}$, $\bar{y}$ and $\bar{z}$ are the CIE standard color matching functions (see Figure 2.3) and Km is the weighing constant (683 lm W^{-1}). From the tristimulus values, the CIE color coordinates calculated by following equations,

$$x = \frac{X}{X+Y+Z} \quad (2.4)$$

$$y = \frac{Y}{X+Y+Z} \quad (2.5)$$

$$z = \frac{Z}{X+Y+Z} \quad (2.6)$$

Any color can be plotted on the CIE chromaticity diagram.

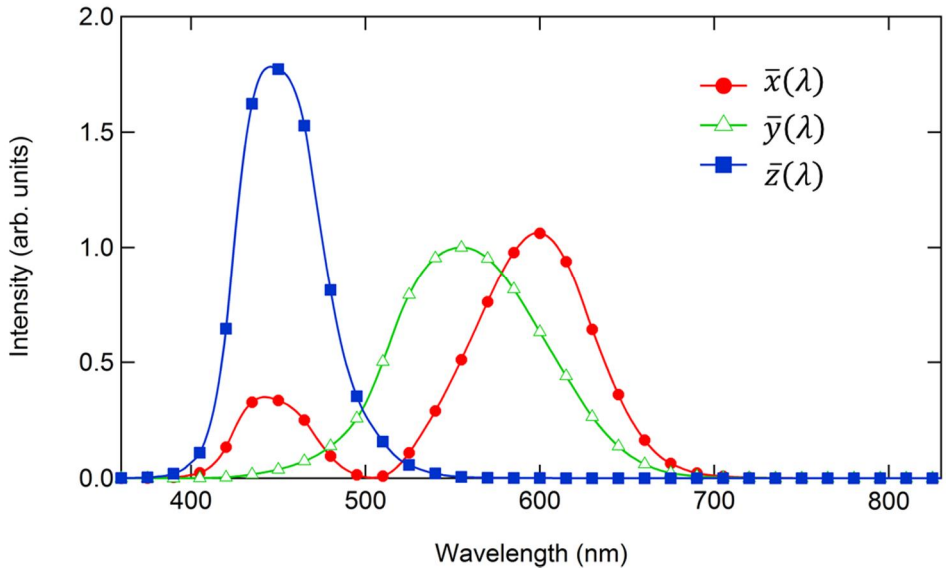

Figure 2.3 The CIE standard observer color matching functions

2.2.3 Efficiency Calculation Methods

To evaluate the emission properties of light-emitting diodes, the commonly employed efficiencies are the external quantum efficiency (EQE), the luminous efficiency (LE) and the power efficiency (PE).

The external quantum efficiency can be defined by the following equation.

$$\mathrm{EQE} = \frac{number\ of\ emitted\ photons}{number\ of\ injected\ electrons}(\%)$$

Typically, QLEDs or OLEDs emit light into the half plane due to the metal contact. Without any modification for increasing out-coupling efficiency, over 80% of the emission can be lost to internal absorption and wave-guiding in a simple planar light-emitting device.

Since human eye has different spectral sensitivity in visible area, the response of the eye is standardized by the CIE in 1924 (see $\bar{y}$ in Figure 2.3). The luminous efficiency weighs all emitted photons according to the photopic response of human eye. The difference is that EQE weighs all emitted photons equally. LE can be expressed by the following equation.

$$\mathrm{LE} = \frac{luminance}{current\ density}(\mathrm{cd\ A^{-1}})$$

The luminance value (cd m^{-2}) can be easily measured by the commercial luminance meter (CS-2000 in this thesis).

The power efficiency is the ratio of the lumen output to the input electrical power as follows,

$$\mathrm{PE} = \frac{luminous\ flux}{electrical\ power}\left(\mathrm{lm\ W^{-1}}\right)$$

The EQEs can be useful to understand the fundamental physics for light emission mechanism, while the PEs can be useful to interpret the power dissipated in a light-emitting device when used in a display application [60].

2.2.4 Other Characterization Methods

Atomic Force Microscopy (AFM): Topography of each film was measured by XE-100 (Park Systems) AFM System. Most of the films were measured in non-contact mode with NCHR probe tip (320 kHz, 42 N m^{-1}) followed by image processing in XEI v.1.7.1.

Film Thickness Measurement: Ellipsometers (L2W15S830 with 632.8-nm He-Ne laser light, Gaertner Scientific Corp. and M2000D, Woollam) and an AFM (XE-100, Park Systems) were used for measuring the thicknesses of films

X-ray Photoelectron Spectroscopy (XPS): Chemical composition of ZnO nanoparticles was characterized by XPS spectrometer (AXIS-HSi, KRATOS).

Steady-State Photoluminescence: PL spectra of QD films were measured by 375-nm laser (iBeam-smart, TOPTICA) and spectrometer (Acton SpectroPro SP-2300, Princeton Instruments).

Device Lifetime Test: Device lifetime tests were conducted with OLED Lifetime Test System (McScience). Constant current corresponding 1000 nit was applied to encapsulated devices.

Chapter 3

Effect of Thermal Annealing on Inverted InP QLEDs

3.1 EL characteristics of thermal annealed inverted InP QLEDs

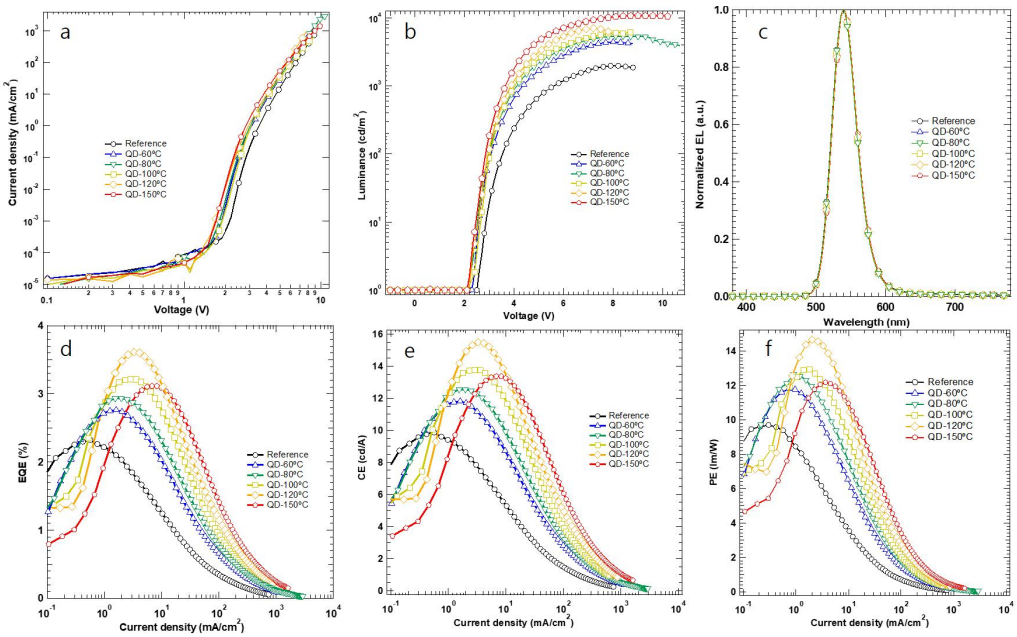

Figure 3.1. (a,b) J-V and L-V characteristics, (c) normalized EL spectra, (d-f) EQE-J, CE-J and PE-J characteristics of the inverted green InP QLEDs with different QD-hotplate-annealing temperatures

QD-hotplate-annealing temperature(℃)	Von (V) (1 cd/m^2)	max EQE (%)	max CE (cd/A)	max PE (lm/W)	max luminance (cd/m^2)
reference	2.5	2.32	9.86	9.69	1960
60	2.3	2.76	11.8	11.78	4390
80	2.2	2.93	12.5	12.64	5350
100	2.2	3.21	13.8	12.92	6170
120	2.2	3.61	15.5	14.65	7710
150	2.2	3.11	13.4	12.18	10700

Table 3.1. Summary of the performance data of the inverted InP QLEDs with different hotplate-annealing temperatures

As described in "Experimental Method" section, inverted green InP QLEDs with and without thermal annealing of InP/ZnSeS/ZnS QDs are demonstrated. Current density-voltage (J-V), luminance-voltage (L-V) characteristics of the reference and QD-annealed QLEDs are shown in Figure 3.1 (a,b). All these characteristics strongly depend on thermal annealing temperature. Leakage current below turn-on voltage is virtually invariant, but beyond turn-on voltage, current density increases and the turn-on voltage (onset of 1 cd/m^2) decreases from 2.5V to 2.2V with higher annealing temperature up to 150℃. Since the layers above InP QDs (HTL/HIL/Al cathode) of the reference and QD-annealed QLEDs are identical, it is reasonable to attribute the changes of J-V characteristics of the InP QLEDs to the improvement of electron transport. According to the previous work, such change of electron transport can either originate from improved conductivity of ZnO NPs or improved electrical contact at the InP QD/ZnO NP interface due to removal of residual solvent and desorption of ligands which are insulating molecules.[56] To investigate the

contribution of ZnO NPs to the enhanced electron transport as thermal annealing, we fabricate electron-only devices (EODs) structured as ITO/ZnO NPs 100nm/Al. ZnO NPs are two-step annealed to account for the first annealing at 100℃ in N_2-filled oven the spin-coating of ZnO NPs and second annealing on hotplate in Ar-filled glovebox right after the spin-coating of InP QDs. In this study, the change in J-V characteristics of annealed QLEDs are well-matched with those of two-step-annealed EODs. The current densities of both QLEDs and EODs increase in the temperature range from 60℃ to 120℃ and decrease in the temperature range from 120℃ to 150℃ as shown in Figure 3.1a and Figure 3.2. It indicates that the improved conductivity of ZnO NPs by additional hotplate-annealing is the major origin of the improved electron transport in the InP QLEDs, and the decaying current density of QD-annealed QLEDs above 150℃ is due to deteriorated stability of ZnO NPs.

Luminance at the same bias voltage monotonically increases with higher annealing temperature as shown in Figure 3.1b. The maximum luminance of 150℃-QD-annealed QLEDs is 10700 cd/m^2 at 9.2V, whereas reference QLEDs have the maximum luminance of 2000 cd/m^2 at 8.0V. Higher luminance with higher annealing temperature can be attributed to both improved electron transport of ZnO NPs raising exciton concentration and PL enhancement of InP QDs. As discussed in the next section, improved electron transport is associated with improved electron mobility of ZnO NPs due to reduced concentration of oxygen vacancies as thermal annealing, which can act as traps. Enhanced PL intensity of InP QDs as thermal annealing is also verified by steady-state PL measurement. Based on the previous studies, it may originate from reduced trap states of QDs and the increased packing density of QDs by removal of residual solvent (toluene) and organic ligands

(1-dodecanethiol).

At the optimal annealing temperature of 120℃, the maximum EQE, CE and PE increase from 2.32%, 9.86 cd/A and 9.69 lm/W to 3.61%, 15.5 cd/A and 14.65 lm/W as shown in Figure 3e-f. Above 120℃, the efficiencies are slightly reduced to 3.11%, 13.4 cd/A and 12.18 lm/W. It is possible that the lowered electron transport of ZnO NPs and the excessive desorption of the organic ligands from InP QDs degrade the QLED efficiencies at such high temperature. The device performances of the InP QLEDs in this work are summarized in Table 1. The major bottleneck of InP QLEDs is widely known as relatively low electron injection/transport due to relatively higher electron injection barrier between InP QDs and commercially available ETLs than the hole injection barrier between InP QDs and HTLs. The improvement of EQE of the inverted InP QLEDs in this study therefore mainly originates from the enhanced charge balance due to increment of electron transport. In addition, the PL enhancement of InP QDs at moderate annealing temperature, also contributes to the raised efficiency. Thermal annealing can thus be an effective and simple way to improve device efficiency.

Figure 3.1c shows EL spectra of the reference and QD-annealed QLEDs with different annealing temperature from 60℃ to 150℃. The InP QLEDs exhibit strong and spectrally pure EL centered at 539 nm with FWHM of 41 nm, and no parasitic emission from organic layers is observed. Any significant spectral shift is observed as thermal annealing, which indicates the chemical composition of InP cores are not affected and aggregation causing redshift of PL does not occur by thermal annealing.

3.2 Effect of thermal annealing on electrical, morphological and photoluminescence characteristics

3.2.1 Origin of improved electron conductivity of ZnO nanoparticles

To unveil the origin of the increased conductivity of ZnO NPs as hotplate thermal annealing, we focus on the shape of the J-V characteristics of two-step annealed EODs as shown in Figure 3.2. Surprisingly, EODs annealed above 100℃ on hotplate exhibit trap-free characteristics whereas EODs annealed below 100℃ have trap charge limited current (TCLC) region at low voltage, indicating that thermal annealing affects trap states of ZnO NPs. Thermal annealing can facilitate diffusion of Zn and O atoms, so the concentration of oxygen vacancy can be changed. Regarding the trap-free characteristics of two-step annealed EODs, it is expected that the concentration of deep traps is lowered by thermal annealing.

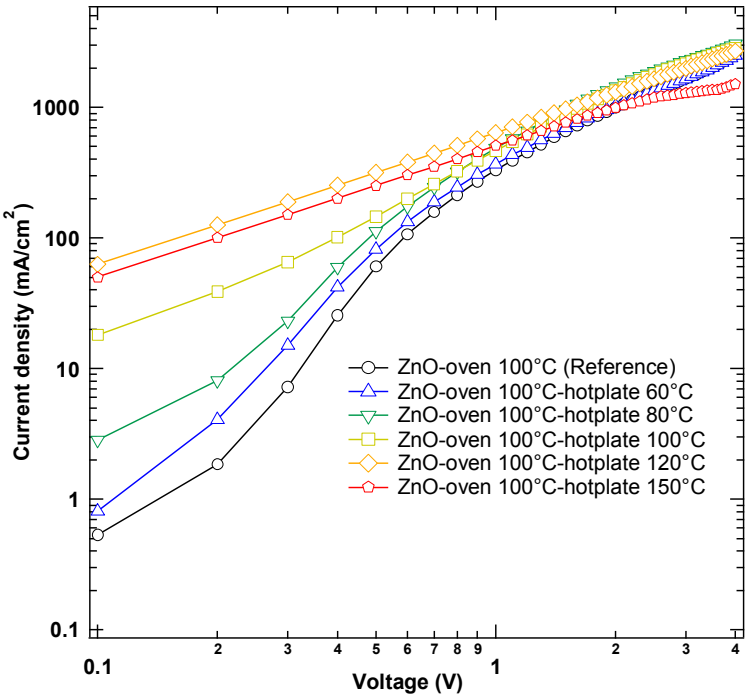

Figure 3.2 J-V characteristics of the EODs (ITO/ZnO NPs 100 nm/Al) annealed with the different second-step hotplate-annealing temperatures for 15 minutes while the first-step annealing is fixed (100℃ N_2-filled oven for 30 minutes)

To characterize the bonding states of annealed ZnO NPs, we use X-ray photoelectron spectroscopy (XPS) of ZnO NPs annealed at different hotplate temperatures. Spin-coated ZnO NPs samples on silicon substrates are also annealed through the two-steps. According to the previous XPS analysis of other groups, O 1s peak of ZnO are decomposed into three Gaussian components corresponding to O-I (oxygen in lattice), O-II (oxygen vacancy) and O-III (oxygen in hydroxide).[51] In our XPS results, O 1s peak is decomposed into two Gaussian components: oxygen in lattice (O-I, centered at 530.3±0.2 eV) and oxygen vacancy (O-II, centered at 531.8±0.2 eV). The O 1s XPS spectra are shown in Figure 3.3. The amount of lattice oxygen

increases from 51.4% to 62.8% and oxygen vacancy decreases from 48.6% to 37.2% as annealing temperature grows up to 150℃. Oxygen vacancies have been known as deep traps with energy level of ~1 eV below conduction band minimum (CBM) in many research groups.[61-62] In this regard, the high concentration of oxygen vacancies as scattering centers can limit electron mobility of ZnO NPs. It is coherent to the trap-free J-V characteristics and high current densities of the two-step annealed EODs with hotplate annealing temperature above 100 ℃. Moreover, the oxygen vacancies as deep traps not only affect the mobility of ZnO NPs but also act as exciton quenchers.[51] Considering that the CBM level of ZnO NPs is ~4.0 eV[39], the traps corresponding to oxygen vacancies have energy levels around 5.0 eV, which is quite close to the VBM level of green InP QDs[8]. Electrons in conduction band (CB) of InP QDs and holes in deep traps of ZnO NPs can therefore recombine (quench) nonradiatively.

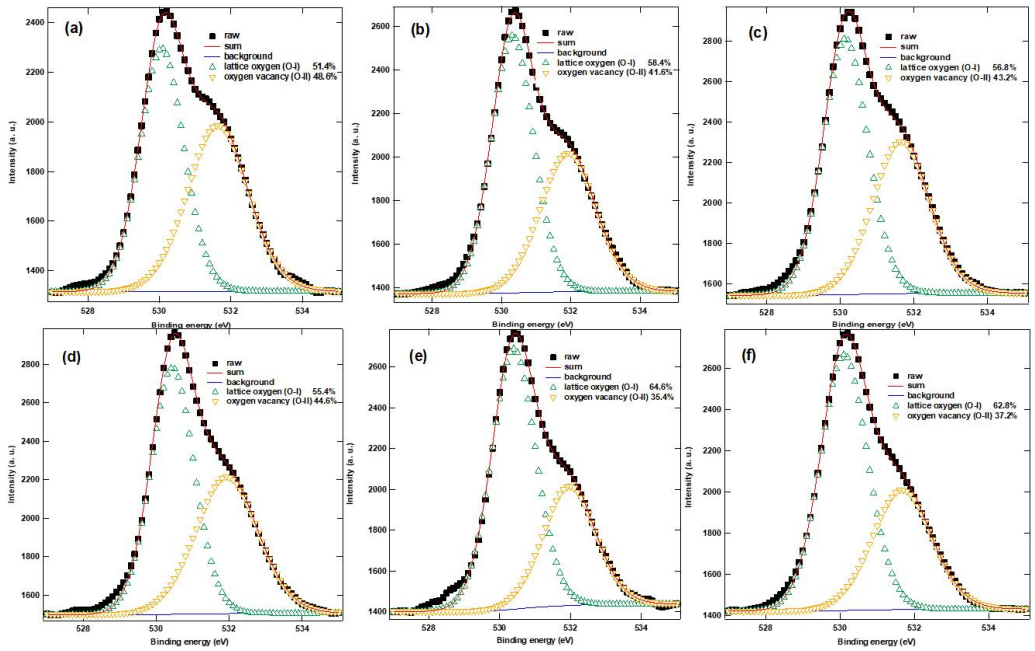

Figure 3.3. O 1s XPS spectra of ZnO NPs annealed with the different

second-step hotplate-annealing temperatures for 15 minutes while the first-step annealing is fixed (100℃ N_2-filled oven for 30 minutes)

3.2.2 Morphologies of InP QDs and the underlying layers

The morphologies of InP QDs and ZnO NPs/PFN with and without thermal annealing on hotplate in Ar-filled glovebox are measured by noncontact-mode atomic force microscopy (AFM) on top of ITO/ZnO NPs/PFN and ITO/ZnO NPs/PFN/QDs where ZnO NPs are oven-annealed right after their spin-coating. The AFM images and topology root-mean-square (RMS) values of QDs and ZnO NPs/PFN are summarized in Figure 3.4, 3.5 and Table 3.2. All samples exhibit quite high film quality with RMS values on the order of 1 nm and no aggregation of InP QDs, and the surface roughness of QDs and ZnO NPs/PFN is not significantly affected by thermal annealing. It is consistent to the almost identical leakage currents of the QD-annealed QLEDs; thermal annealing does not change physical pathways of leakage current. No aggregation is observed in the AFM images, which is also consistent to the invariant PL peak wavelength under thermal annealing. Therefore, any morphological change affected the device performance in this work.

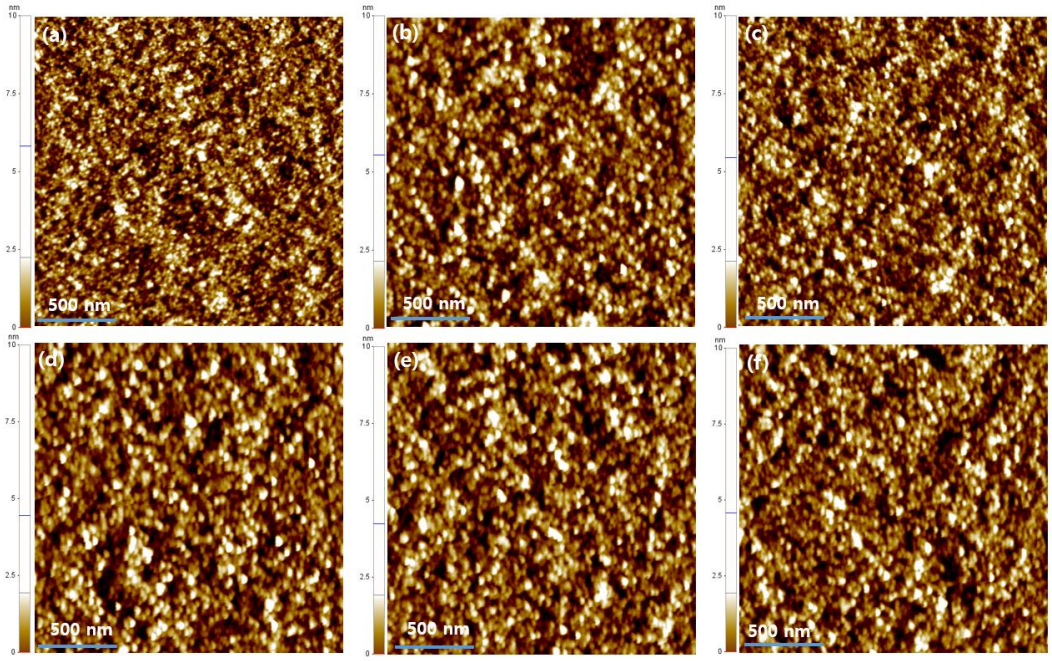

Figure 3.4. AFM topology images of the PFN thin films (a) without hotplate annealing and with hotplate annealing at (b) 60℃ (c) 80℃ (d) 100℃ (e) 120℃ (f) 150℃ on top of 100℃ N_2-filled oven-annealed ITO/ZnO NPs. Scale size: 2μm × 2μm

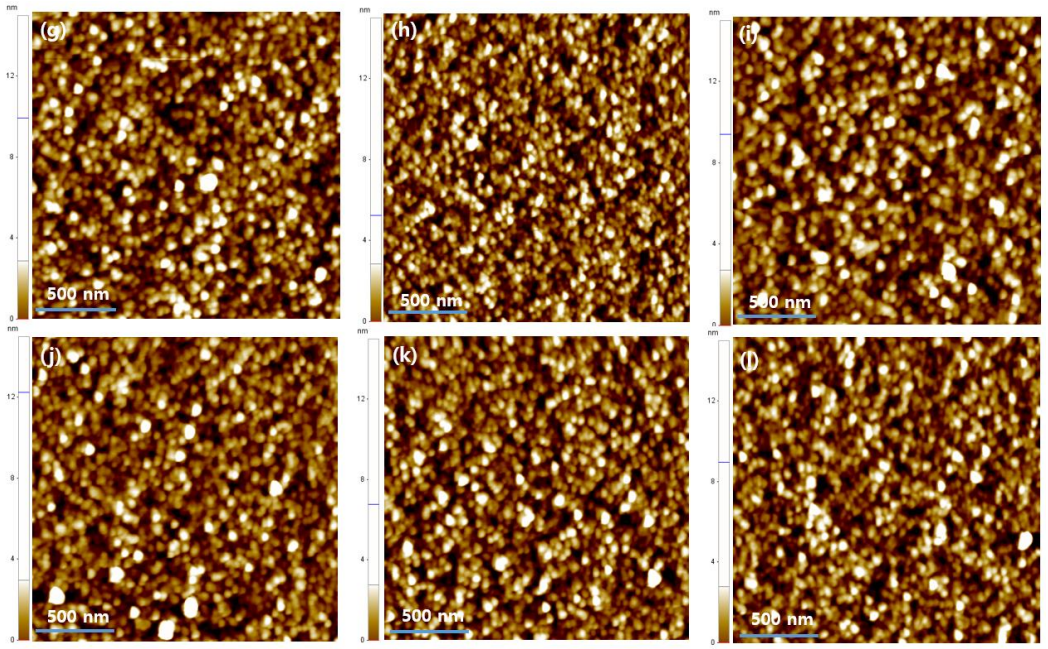

Figure 3.5. AFM topology images of the InP QD thin films (a) without hotplate annealing and with hotplate annealing at (b) 60℃ (c) 80℃ (d) 100℃ (e) 120℃ (f) 150℃ on top of 100℃ N_2-filled oven-annealed ITO/ZnO NPs. Scale size: 2μm × 2μm

In the previous work of A. Jen's group, they also observed enhanced current, luminance and efficiency after thermal annealing QDs (CdSe/CdS QDs in their work). However, they observed noticeable smoothening of QDs after thermal annealing contributing device improvement. Such difference between A. Jen's work and this thesis originates from the distinct device structure. In A. Jen's work, the device architecture was normal-type. QDs were thus deposited on HTL, BiVB-MeTPD, which is cross-linkable molecule. Although roughness of BiVB-MeTPD was very low as 0.563 nm, but the roughness right after spin-coating CdSe/CdS QDs increased to 2.57 nm. Such high roughness can originate from bad wettability or too thin QD layers (~1ML). In this regard, there was a loom for improving quality of QD thin films by thermal annealing. In this thesis, however, InP QDs are well-coated and well-packed on ZnO NPs, so morphological change is not exhibited by thermal annealing.

sample	hotplate-annealing temperature (℃)	RMS value (nm)
ITO/ZnO NPs/PFN	oven-only	1.11
	60	1.05
	80	1.05
	100	0.949

	120	0.953
	150	0.939
ITO/ZnO NPs/PFN/QDs	oven-only	1.40
	60	1.40
	80	1.33
	100	1.45
	120	1.35
	150	1.37

Table 3.2. AFM data of the surface of PFN and InP QDs on top of 100℃ N_2-filled oven-annealed ITO/ZnO NPs with and without hotplate annealing at different temperatures

3.2.3 Photoluminescence of InP QDs

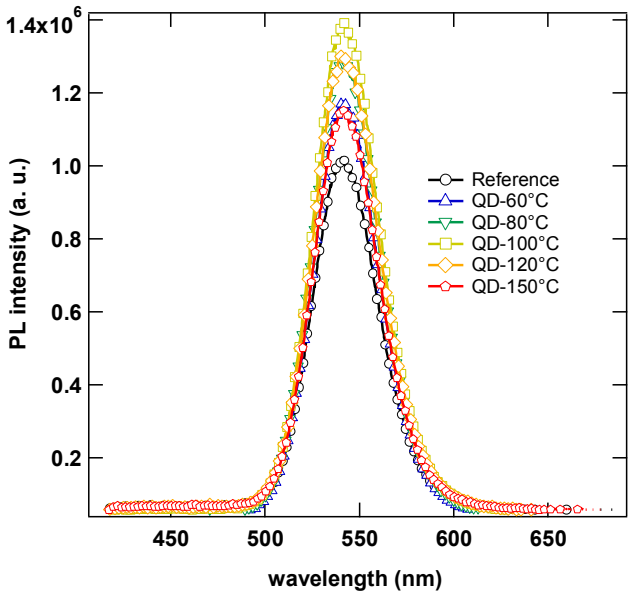

Figure 3.6. PL spectra of InP QD thin films with different hotplate-annealing temperatures

The effect of thermal annealing on PL characteristics of the InP QDs is studied by steady-state PL measurements. Spin-coated InP QDs samples on glass substrate are heated at the preset temperatures (60, 80, 100, 120 and 150℃) on hotplates in Ar-filled glovebox for 15 minutes. The PL spectra of the InP QDs excited by 375-nm laser as a function of annealing temperature are shown in Figure 3.6. The PL intensity of InP QDs is noticeably enhanced by 36% after thermal annealing at 100 ℃. It can be attributed to reduced trap states of InP QDs and increased packing density due to ligand desorption.[57] Beyond 100℃, the PL intensity is drastically degraded as the thermal degradation process of ligands and surface defects get over the thermal enhancement process of alleviation of defects and removal of residual solvents and impurities.[56] Similar to the EL spectra as a function of annealing temperature, no spectral shift is observed for the PL spectra of InP QDs as thermal annealing.

The tendency of PL intensity of InP QDs as a function of thermal annealing temperature is opposite to that of CdSe/CdS QDs in A. Jen's work. They obtained decreasing PL efficiency with annealing temperature from 80 ℃ to 140 ℃. Same tendency with solid-state CdSe/CdS QDs was observed by K. Gong's group.[63] Several spectroscopic measurements implied that the lattice strain release at CdSe/CdS interface via thermal annealing can create hole traps near the valence band of CdSe. The opposite result with thermal annealed InP/ZnSeS/ZnS QDs thus indicate that the hole traps at InP/ZnSe interface may be eliminated by thermal annealing. Since adjacent ZnO NPs also have trap states near the valence band of InP QDs, the effect of thermal annealing on trap states of InP QDs are expected to be significant in QLEDs.

3.3 Device stability of thermal annealed inverted InP QLEDs

3.3.1 Lifetime

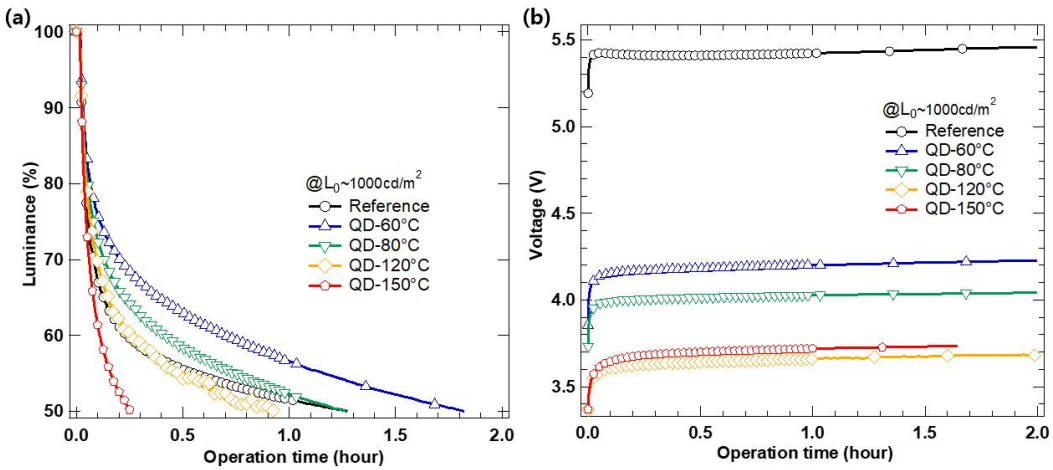

Figure 3.7. (a) Luminance-time (b) voltage-time characteristics of the QD-annealed QLEDs driven by constant current with initial luminance around 1000 cd/m^2

In addition to the enhancement in efficiency and luminance, device stability of the QLEDs is also strongly dependent on annealing temperature of QDs.

The QLEDs are encapsulated with UV-curable resin in Ar-filled glovebox and driven at constant currents with initial luminance (L_0) around 1000 cd/m^2 under ambient atmosphere condition. Figure 3.7 shows the luminance-time and voltage-time characteristics of the QLEDs with different annealing temperature under constant current condition with the initial luminance of around 1000 cd/m^2. 60℃-QD-annealed QLEDs show the longest half-lifetime (T_{50}), 1.85 h at the initial luminance of 1040 cd/m^2. It is 1.47-fold improvement compared to the reference QLEDs which show half-lifetime of 1.26 h at the initial luminance of 994 cd/m^2. Assuming the empirical relationship, $L_0^n T_{50} = \text{const}$ with n=1.5, the half-lifetime at the initial luminance of 100 cd/m^2 is expected to be 62.0 h. As far as I know, it is the longest lifetime of InP QLEDs reported so far.

The initial luminance loss is so rapid that T_{90} is around 2 minutes which is almost identical for all the driven QLEDs regardless of annealing temperature. According to the recent discovery of degradation mechanisms of QLEDs[64], the initial luminance decay is classified as "Phase 1 degradation." Loss of luminance is mainly due to charging of QDs. It can be deduced from the results here that the electron injection barrier is still high despite the introduction of PFN dipole layers and the barrier does not change by thermal annealing. The QD-annealed QLEDs annealed at 60℃ and 80℃ undergo less luminance loss between T_{90} and T_{50} than the reference QLED. This range corresponds to "Phase 2 degradation," which is relevant to permanent degradation of organic HTL. In particular, T_{50} of the reference and 80℃-QD-annealed QLED are very similar, but the luminance loss before T_{50} of 80℃-QD annealed QLED is less than that of the reference QLED. The distinct shape of luminance decay curves with different annealing

temperatures imply that degradation mechanisms may differ for the reference and QD-annealed QLEDs. In contrast to the efficiency which is enhanced up to 120℃, it is noticeable that the optimal annealing temperature is less than 120℃. The enhanced efficiency originates from the increased conductivity of ZnO NPs and improved PL intensity of InP QDs as annealing, but thermal annealing of may deteriorate long-term stability of ZnO NPs and InP QDs.

3.4 Summary

The QLEDs are structured as inverted architecture of glass/ITO 150 nm (cathode)/ZnO nanoparticles 40 nm (ZnO NPs, ETL)/poly [(9,9-bis(3'-(N,N-dimethylamino)propyl)-2,7-fluorene)-alt-2,7-(9,9–dioctylfluorene)] (PFN-P1, surface modifying layer)/green InP/ZnSeS/ZnS core/shell QDs 16 nm (InP QDs, EML)/tris(4-carbazoyl-9-ylphenyl)amine 50 nm (TCTA, HTL)/ MoO_3 10 nm (hole injection layer, HIL)/Al 130 nm (anode). ZnO NPs, PFN-P1 and green InP QDs are spin-coated and the upper layers are thermally vacuum deposited at high vacuum below 10^{-6} Torr. The green InP QDs have InP cores and multilayer ZnSeS/ZnS alloyed shells with compositional gradient, and their average diameter is around 7 nm. The InP QDs are dispersed in toluene, and passivated by 1-dodecanethiol (DDT) ligands.

Here, hotplate thermal annealing with different temperatures (60, 80, 100, 120 and 150℃) for 15 minutes is applied to ITO/ZnO NPs/PFN/InP QDs right after the spin-coating of InP QDs, so InP QDs are annealed once while ZnO NPs are annealed by two-steps: 100℃ N_2-filled oven-annealing for 30 minutes right after the spin-coating of ZnO NPs and hotplate-annealing for 15 minutes in Ar-filled glovebox right after the spin-coating of InP QDs. The

electrical, optical and morphological effects of the hotplate thermal annealing on inverted InP QLEDs are investigated. InP QLEDs without thermal annealing of QDs are named as reference devices and those with annealed QDs are noted as QD-annealed devices, and the annealing temperatures refer to the hotplate-annealing temperatures in this paper.

Conclusion

In this work, we demonstrate that thermal annealing InP QDs and the underlying layers can be an effective and simple method to improve the performance of inverted InP QLEDs. Annealing the ETL and EML of the inverted InP QLEDs at 120℃ enhances the peak EQE to 3.61% which is 1.56-fold improvement compared to the reference QLEDs. The optimum half-lifetime is 1.85 h at the initial luminance of 1040 cd/m^2 at the lower annealing temperature, 60℃. The converted half-lifetime at the initial luminance of 100 cd/m^2 is 62.0 h which is the record-breaking lifetime of InP QLEDs. The mechanisms of EL enhancement of the inverted InP QLEDs via thermal annealing ZnO NPs/InP QDs layers are studied by analyzing the electrical, optical and morphological changes of ZnO NPs and InP QDs. The main origins of the efficiency enhancement are attributed to (i) the improved charge balance due to increased electron transport from ZnO NPs ETL to InP QDs EML, (ii) reduced exciton quenching between InP QDs and ZnO NPs and (iii) the improved PL intensity of InP QD thin films. Thermal annealing

reduces oxygen vacancies which can act as scattering sites of ZnO NPs, so the electron mobility of ZnO NPs increases and the exciton quenching at the InP QDs/ZnO NPs interface may be suppressed. Annealing process can also effectively remove the residual solvents, insulating organic ligands and impurities in solution-processed InP QDs, and can alleviate the surface defects of InP QDs, so the PL efficiency of InP QDs EML increases up to the optimal annealing temperature. The removal of residual solvents may lead more densely packed InP QDs, which can cause the increased PL intensity per unit area. Thermal annealing of InP QDs can therefore be a simple and practical process to further optimize inverted InP QLEDs.

Bibilography

1. Peng, H.; Jiang, Y.; Chen, S., Efficient vacuum-free-processed quantum dot light-emitting diodes with printable liquid metal cathodes. *Nanoscale* **2016,** *8* (41), 17765-17773.

2. Dai, X.; Zhang, Z.; Jin, Y.; Niu, Y.; Cao, H.; Liang, X.; Chen, L.; Wang, J.; Peng, X., Solution-processed, high-performance light-emitting diodes based on quantum dots. *Nature* **2014,** *515* (7525), 96-9.

3. Acharya, K. P.; Titov, A.; Hyvonen, J.; Wang, C.; Tokarz, J.; Holloway, P. H., High efficiency quantum dot light emitting diodes from positive aging. *Nanoscale* **2017,** *9* (38), 14451-14457.

4. Wang, L.; Lin, J.; Hu, Y.; Guo, X.; Lv, Y.; Tang, Z.; Zhao, J.; Fan, Y.; Zhang, N.; Wang, Y.; Liu, X., Blue Quantum Dot Light-Emitting Diodes

with High Electroluminescent Efficiency. *ACS Appl Mater Interfaces* **2017,** *9* (44), 38755-38760.

5. Lim, J.; Park, Y. S.; Wu, K.; Yun, H. J.; Klimov, V. I., Droop-Free Colloidal Quantum Dot Light-Emitting Diodes. *Nano Lett* **2018,** *18* (10), 6645-6653.

6. Li, Z.; Hu, Y.; Shen, H.; Lin, Q.; Wang, L.; Wang, H.; Zhao, W.; Li, Lin S., Efficient and long-life green light-emitting diodes comprising tridentate thiol capped quantum dots. *Laser & Photonics Reviews* **2017,** *11* (1).

7. Yang, Y.; Zheng, Y.; Cao, W.; Titov, A.; Hyvonen, J.; Manders, J. R.; Xue, J.; Holloway, P. H.; Qian, L., High-efficiency light-emitting devices based on quantum dots with tailored nanostructures. *Nature Photonics* **2015,** *9* (4), 259-266.

8. Kochuveedu, S. T.; Son, T.; Lee, Y.; Lee, M.; Kim, D.; Kim, D. H., Revolutionizing the FRET-based light emission in core-shell nanostructures via comprehensive activity of surface plasmons. *Sci Rep* **2014,** *4*, 4735.

9. Coropceanu, I.; Bawendi, M. G., Core/shell quantum dot based luminescent solar concentrators with reduced reabsorption and enhanced efficiency. *Nano Lett* **2014,** *14* (7), 4097-101.

10. Ippen, C.; Greco, T.; Kim, Y.; Pries, C.; Kim, J.; Oh, M. S.; Han, C. J.; Wedel, A., Color tuning of indium phosphide quantum dots for cadmium-free quantum dot light-emitting devices with high efficiency and color saturation. *Journal of the Society for Information Display* **2015,** *23* (7), 285-293.

11. Jang, I.; Kim, J.; Park, C. J.; Ippen, C.; Greco, T.; Oh, M. S.; Lee, J.; Kim, W. K.; Wedel, A.; Han, C. J.; Park, S. K., Study of ethanolamine surface treatment on the metal-oxide electron transport layer in inverted InP quantum

dot light-emitting diodes. *Electronic Materials Letters* **2015,** *11* (6), 1066-1071.

12. Jo, J. H.; Kim, J. H.; Lee, K. H.; Han, C. Y.; Jang, E. P.; Do, Y. R.; Yang, H., High-efficiency red electroluminescent device based on multishelled InP quantum dots. *Opt Lett* **2016,** *41* (17), 3984-7.

13. Kim, H. Y.; Park, Y. J.; Kim, J.; Han, C. J.; Lee, J.; Kim, Y.; Greco, T.; Ippen, C.; Wedel, A.; Ju, B.-K.; Oh, M. S., Transparent InP Quantum Dot Light-Emitting Diodes with ZrO2Electron Transport Layer and Indium Zinc Oxide Top Electrode. *Advanced Functional Materials* **2016,** *26* (20), 3454-3461.

14. Kim, J.-W.; Kim, J., Flexible InP based quantum dot light-emitting diodes using Ag nanowire-colorless polyimide composite electrode. *Journal of Vacuum Science & Technology B, Nanotechnology and Microelectronics: Materials, Processing, Measurement, and Phenomena* **2017,** *35* (4).

15. Kim, Y.; Ippen, C.; Fischer, B.; Lange, A.; Wedel, A., Efficiency enhancement of InP-based inverted QD-LEDs by incorporation of a polyethylenimine modified Al:ZnO layer. *Journal of the Society for Information Display* **2015,** *23* (8), 377-383.

16. Kuo, T. R.; Hung, S. T.; Lin, Y. T.; Chou, T. L.; Kuo, M. C.; Kuo, Y. P.; Chen, C. C., Green Synthesis of InP/ZnS Core/Shell Quantum Dots for Application in Heavy-Metal-Free Light-Emitting Diodes. *Nanoscale Res Lett* **2017,** *12* (1), 537.

17. Lim, J.; Bae, W. K.; Lee, D.; Nam, M. K.; Jung, J.; Lee, C.; Char, K.; Lee, S., InP@ZnSeS, Core@Composition Gradient Shell Quantum Dots with Enhanced Stability. *Chemistry of Materials* **2011,** *23* (20), 4459-4463.

18. Shen, W.; Tang, H.; Yang, X.; Cao, Z.; Cheng, T.; Wang, X.; Tan, Z.; You, J.; Deng, Z., Synthesis of highly fluorescent InP/ZnS small-core/thick-

shell tetrahedral-shaped quantum dots for blue light-emitting diodes. *Journal of Materials Chemistry C* **2017,** *5* (32), 8243-8249.

19. Wang, H. C.; Zhang, H.; Chen, H. Y.; Yeh, H. C.; Tseng, M. R.; Chung, R. J.; Chen, S.; Liu, R. S., Cadmium-Free InP/ZnSeS/ZnS Heterostructure-Based Quantum Dot Light-Emitting Diodes with a ZnMgO Electron Transport Layer and a Brightness of Over 10 000 cd m(-2). *Small* **2017,** *13* (13).

20. Yang, X.; Zhao, D.; Leck, K. S.; Tan, S. T.; Tang, Y. X.; Zhao, J.; Demir, H. V.; Sun, X. W., Full visible range covering InP/ZnS nanocrystals with high photometric performance and their application to white quantum dot light-emitting diodes. *Adv Mater* **2012,** *24* (30), 4180-5.

21. Dey, S. C.; Nath, S. S., Electroluminescence of colloidal ZnSe quantum dots. *Journal of Luminescence* **2011,** *131* (12), 2707-2710.

22. Ippen, C.; Greco, T.; Kim, Y.; Kim, J.; Oh, M. S.; Han, C. J.; Wedel, A., ZnSe/ZnS quantum dots as emitting material in blue QD-LEDs with narrow emission peak and wavelength tunability. *Organic Electronics* **2014,** *15* (1), 126-131.

23. Ji, W.; Jing, P.; Xu, W.; Yuan, X.; Wang, Y.; Zhao, J.; Jen, A. K. Y., High color purity ZnSe/ZnS core/shell quantum dot based blue light emitting diodes with an inverted device structure. *Applied Physics Letters* **2013,** *103* (5).

24. Wang, A.; Shen, H.; Zang, S.; Lin, Q.; Wang, H.; Qian, L.; Niu, J.; Song Li, L., Bright, efficient, and color-stable violet ZnSe-based quantum dot light-emitting diodes. *Nanoscale* **2015,** *7* (7), 2951-9.

25. Xiang, C.; Koo, W.; Chen, S.; So, F.; Liu, X.; Kong, X.; Wang, Y., Solution processed multilayer cadmium-free blue/violet emitting quantum dots light emitting diodes. *Applied Physics Letters* **2012,** *101* (5).

26. Chen, B.; Zhong, H.; Zhang, W.; Tan, Z. a.; Li, Y.; Yu, C.; Zhai, T.; Bando, Y.; Yang, S.; Zou, B., Highly Emissive and Color-Tunable CuInS2-Based Colloidal Semiconductor Nanocrystals: Off-Stoichiometry Effects and Improved Electroluminescence Performance. *Advanced Functional Materials* **2012,** *22* (10), 2081-2088.

27. Kim, J.-H.; Han, C.-Y.; Lee, K.-H.; An, K.-S.; Song, W.; Kim, J.; Oh, M. S.; Do, Y. R.; Yang, H., Performance Improvement of Quantum Dot-Light-Emitting Diodes Enabled by an Alloyed ZnMgO Nanoparticle Electron Transport Layer. *Chemistry of Materials* **2014,** *27* (1), 197-204.

28. Kim, J.-H.; Lee, K.-H.; Jo, D.-Y.; Lee, Y.; Hwang, J. Y.; Yang, H., Cu−In−Ga−S quantum dot composition-dependent device performance of electrically driven light-emitting diodes. *Applied Physics Letters* **2014,** *105* (13).

29. Li, J.; Jin, H.; Wang, K.; Xie, D.; Xu, D.; Xu, X.; Xu, G., High luminance of CuInS2-based yellow quantum dot light emitting diodes fabricated by all-solution processing. *RSC Advances* **2016,** *6* (76), 72462-72470.

30. Tan, Z.; Zhang, Y.; Xie, C.; Su, H.; Liu, J.; Zhang, C.; Dellas, N.; Mohney, S. E.; Wang, Y.; Wang, J.; Xu, J., Near-band-edge electroluminescence from heavy-metal-free colloidal quantum dots. *Adv Mater* **2011,** *23* (31), 3553-8.

31. Zhang, W.; Lou, Q.; Ji, W.; Zhao, J.; Zhong, X., Color-Tunable Highly Bright Photoluminescence of Cadmium-Free Cu-Doped Zn–In–S Nanocrystals and Electroluminescence. *Chemistry of Materials* **2013,** *26* (2), 1204-1212.

32. Zhang, Y.; Xie, C.; Su, H.; Liu, J.; Pickering, S.; Wang, Y.; Yu, W. W.; Wang, J.; Wang, Y.; Hahm, J. I.; Dellas, N.; Mohney, S. E.; Xu, J.,

Employing heavy metal-free colloidal quantum dots in solution-processed white light-emitting diodes. *Nano Lett* **2011,** *11* (2), 329-32.

33. Zhong, H.; Wang, Z.; Bovero, E.; Lu, Z.; van Veggel, F. C. J. M.; Scholes, G. D., Colloidal CuInSe2 Nanocrystals in the Quantum Confinement Regime: Synthesis, Optical Properties, and Electroluminescence. *The Journal of Physical Chemistry C* **2011,** *115* (25), 12396-12402.

34. Bhaumik, S.; Pal, A. J., Light-emitting diodes based on solution-processed nontoxic quantum dots: oxides as carrier-transport layers and introducing molybdenum oxide nanoparticles as a hole-inject layer. *ACS Appl Mater Interfaces* **2014,** *6* (14), 11348-56.

35. Choi, D. B.; Kim, S.; Yoon, H. C.; Ko, M.; Yang, H.; Do, Y. R., Color-tunable Ag-In-Zn-S quantum-dot light-emitting devices realizing green, yellow and amber emissions. *Journal of Materials Chemistry C* **2017,** *5* (4), 953-959.

36. Ji, C.; Lu, M.; Wu, H.; Zhang, X.; Shen, X.; Wang, X.; Zhang, Y.; Wang, Y.; Yu, W. W., 1,2-Ethanedithiol Treatment for AgIn5S8/ZnS Quantum Dot Light-Emitting Diodes with High Brightness. *ACS Appl Mater Interfaces* **2017,** *9* (9), 8187-8193.

37. Fuhr, A. S.; Yun, H. J.; Makarov, N. S.; Li, H.; McDaniel, H.; Klimov, V. I., Light Emission Mechanisms in CuInS2 Quantum Dots Evaluated by Spectral Electrochemistry. *ACS Photonics* **2017,** *4* (10), 2425-2435.

38. Bae, W. K.; Park, Y. S.; Lim, J.; Lee, D.; Padilha, L. A.; McDaniel, H.; Robel, I.; Lee, C.; Pietryga, J. M.; Klimov, V. I., Controlling the influence of Auger recombination on the performance of quantum-dot light-emitting diodes. *Nat Commun* **2013,** *4*, 2661.

39. Kwak, J.; Bae, W. K.; Lee, D.; Park, I.; Lim, J.; Park, M.; Cho, H.; Woo, H.; Yoon, D. Y.; Char, K.; Lee, S.; Lee, C., Bright and efficient full-color colloidal quantum dot light-emitting diodes using an inverted device structure. *Nano Lett* **2012,** *12* (5), 2362-6.

40. Shen, H.; Lin, Q.; Wang, H.; Qian, L.; Yang, Y.; Titov, A.; Hyvonen, J.; Zheng, Y.; Li, L. S., Efficient and bright colloidal quantum dot light-emitting diodes via controlling the shell thickness of quantum dots. *ACS Appl Mater Interfaces* **2013,** *5* (22), 12011-6.

41. Beane, G. A.; Gong, K.; Kelley, D. F., Auger and Carrier Trapping Dynamics in Core/Shell Quantum Dots Having Sharp and Alloyed Interfaces. *ACS Nano* **2016,** *10* (3), 3755-65.

42. Park, Y. S.; Lim, J.; Makarov, N. S.; Klimov, V. I., Effect of Interfacial Alloying versus "Volume Scaling" on Auger Recombination in Compositionally Graded Semiconductor Quantum Dots. *Nano Lett* **2017,** *17* (9), 5607-5613.

43. Park, Y. S.; Bae, W. K.; Padilha, L. A.; Pietryga, J. M.; Klimov, V. I., Effect of the core/shell interface on auger recombination evaluated by single-quantum-dot spectroscopy. *Nano Lett* **2014,** *14* (2), 396-402.

44. Fukuda, T.; Hishinuma, M.; Maki, J.; Sasaki, H., Quantum Dot Light-Emitting Diode with Ligand-Exchanged ZnCuInS Quantum Dot. *IEICE Transactions on Electronics* **2017,** *E100.C* (11), 943-948.

45. Kim, D.; Fu, Y.; Kim, J.; Lee, K. H.; Kim, H.; Yang, H.; Chae, H., Improved electroluminescence of quantum dot light-emitting diodes enabled by a partial ligand exchange with benzenethiol. *Nanotechnology* **2016,** *27* (24), 245203.

46. Liu, I. S.; Lo, H.-H.; Chien, C.-T.; Lin, Y.-Y.; Chen, C.-W.; Chen, Y.-F.; Su, W.-F.; Liou, S.-C., Enhancing photoluminescence quenching and

photoelectric properties of CdSe quantum dots with hole accepting ligands. *Journal of Materials Chemistry* **2008,** *18* (6).

47. Cao, S.; Zheng, J.; Zhao, J.; Yang, Z.; Li, C.; Guan, X.; Yang, W.; Shang, M.; Wu, T., Enhancing the Performance of Quantum Dot Light-Emitting Diodes Using Room-Temperature-Processed Ga-Doped ZnO Nanoparticles as the Electron Transport Layer. *ACS Appl Mater Interfaces* **2017,** *9* (18), 15605-15614.

48. Ho, M. D.; Kim, D.; Kim, N.; Cho, S. M.; Chae, H., Polymer and small molecule mixture for organic hole transport layers in quantum dot light-emitting diodes. *ACS Appl Mater Interfaces* **2013,** *5* (23), 12369-74.

49. Kim, H.-M.; bin Mohd Yusoff, A. R.; Youn, J.-H.; Jang, J., Inverted quantum-dot light emitting diodes with cesium carbonate doped aluminium-zinc-oxide as the cathode buffer layer for high brightness. *Journal of Materials Chemistry C* **2013,** *1* (25).

50. Kim, H.-M.; Youn, J.-H.; Seo, G.-J.; Jang, J., Inverted quantum-dot light-emitting diodes with solution-processed aluminium–zinc oxide as a cathode buffer. *J. Mater. Chem. C* **2013,** *1* (8), 1567-1573.

51. Sun, Y.; Jiang, Y.; Peng, H.; Wei, J.; Zhang, S.; Chen, S., Efficient quantum dot light-emitting diodes with a Zn0.85Mg0.15O interfacial modification layer. *Nanoscale* **2017,** *9* (26), 8962-8969.

52. Sun, Y.; Wang, W.; Zhang, H.; Su, Q.; Wei, J.; Liu, P.; Chen, S.; Zhang, S., High-Performance Quantum Dot Light-Emitting Diodes Based on Al-Doped ZnO Nanoparticles Electron Transport Layer. *ACS Appl Mater Interfaces* **2018,** *10* (22), 18902-18909.

53. Wang, L.; Chen, T.; Lin, Q.; Shen, H.; Wang, A.; Wang, H.; Li, C.; Li, L. S., High-performance azure blue quantum dot light-emitting diodes via doping PVK in emitting layer. *Organic Electronics* **2016,** *37*, 280-286.

54. Zuo, L.; Zhang, S.; Dai, S.; Chen, H., Versatility and robustness of ZnO:Cs electron transporting layer for printable organic solar cells. *RSC Advances* **2015,** *5* (61), 49369-49375.

55. Kim, K.; Woo, J. Y.; Jeong, S.; Han, C. S., Photoenhancement of a quantum dot nanocomposite via UV annealing and its application to white LEDs. *Adv Mater* **2011,** *23* (7), 911-4.

56. Niu, Y. H.; Munro, A. M.; Cheng, Y. J.; Tian, Y. Q.; Liu, M. S.; Zhao, J. L.; Bardecker, J. A.; Jen-La Plante, I.; Ginger, D. S.; Jen, A. K. Y., Improved Performance from Multilayer Quantum Dot Light-Emitting Diodes via Thermal Annealing of the Quantum Dot Layer. *Advanced Materials* **2007,** *19* (20), 3371-3376.

57. Tetsuka, H.; Ebina, T.; Mizukami, F., Highly Luminescent Flexible Quantum Dot-Clay Films. *Advanced Materials* **2008,** *20* (16), 3039-3043.

58. Fu, Y.; Kim, D.; Moon, H.; Yang, H.; Chae, H., Hexamethyldisilazane-mediated, full-solution-processed inverted quantum dot-light-emitting diodes. *Journal of Materials Chemistry C* **2017,** *5* (3), 522-526.

59. Pacholski, C.; Kornowski, A.; Weller, H., Self-Assembly of ZnO: From Nanodots to Nanorods. *Angew. Chem., Int. Ed.* **2002,** *41* (7), 1188-1191.

60. Forrest, S. R.; Bradley, D. D. C.; Thompson, M. E., Measuring the Efficiency of Organic Light-Emitting Devices. *Adv. Mater.* **2003,** *15* (13), 1043-1048.

61. Janotti, A.; Van de Walle, C. G., Fundamentals of zinc oxide as a semiconductor. *Reports on Progress in Physics* **2009,** *72* (12).

62. Janotti, A.; Van de Walle, C. G., Oxygen vacancies in ZnO. *Applied Physics Letters* **2005,** *87* (12).

63. Gong, K.; Beane, G.; Kelley, D. F., Strain Release in Metastable CdSe/CdS Quantum Dots. *Chem Phys* **2015,** *471* (1), 6.

64. Chang, J. H.; Park, P.; Jung, H.; Jeong, B. G.; Hahm, D.; Nagamine, G.; Ko, J.; Cho, J.; Padilha, L. A.; Lee, D. C.; Lee, C.; Char, K.; Bae, W. K., Unraveling the Origin of Operational Instability of Quantum Dot Based Light-Emitting Diodes. *ACS Nano* **2018,** *12* (10), 10231-10239.

한글 초록

인화인듐 양자점은 비카드뮴계 양자점 발광다이오드를 위한 유망한 소재로 각광받고 있다. 그러나 현재로서는 효율, 휘도, 수명 측면에서 인화인듐 양자점 발광다이오드는 카드뮴계 양자점 발광다이오드보다 성능이 크게 떨어진다. 이는 주로 인화인듐 양자점의 나노구조와 발광다이오드 소자구조가 충분히 최적화되지 않은데에 기인한다. 인화인듐 양자점은 상대적으로 작은 전자친화도를 가지므로 일반적으로 사용하는 전자수송재료와의 전자 주입장벽이 커서 전자 주입 및 수송이 제한적이다. 본 논문에서는 전자수송재료인 산화아연 나노입자와 인화인듐 양자점을 간단히 열처리 함으로써 공정의 복잡도를 증가시키지 않고 전자수송 특성을 개선하여 인화인듐 양자점 발광다이오드의 성능을 향상시킬 수 있음을 보였다. 또한 산화아연 나노입자와 전극으로 구성된 단일 전자 소자를 제작하여 열처리에 따른 산화아연 나노입자의 전도도 향상이 소자 내 전류 증가의 주요한

원인임을 밝히고, 특정 온도 이상에서 열처리 시 산화아연 나노입자의 트랩 무관 전도특성을 보임을 확인하였다. 이는 전하 나르개 및 엑시톤을 산란시킬 수 있는 산화아연 나노입자의 산소공백이 열처리에 따라 줄어들기 때문이다. 게다가 인화인듐 양자점 박막의 발광 세기가 열처리에 따라 특정온도까지 증가하는 현상이 관찰되었는데, 이는 인화인듐 양자점의 트랩농도가 열처리에 따라 감소하거나 양자점 박막의 조밀도가 증가하기 때문으로 생각된다.

열처리 온도를 최적화한 결과, 역구조 녹색 인화인듐 양자점 발광다이오드의 외부양자효율을 2.32%에서 3.61%까지 증가시키고 최대휘도를 10,000 cd/m^2로 증가시켰으며, 100 cd/m^2 기준 반감수명을 학계 최장인 62시간을 달성할 수 있었다. 결론적으로 본 연구에서 논의된 양자점과 산화아연 전하수송층의 열처리가 역구조 인화인듐 양자점 발광다이오드의 성능 향상에 간단하면서도 효과적으로 이용될 수 있다고 생각된다.

주요어: 인화인듐 양자점, 양자점 발광다이오드, 열처리, 산화아연 나노입자, 산소공백, 전하균형
학번: 2017-28685